Electronic Structure, Ionization Potential, and Electron Affinity of the Enzyme Cofactor (6*R*)-5,6,7,8-Tetrahydrobiopterin in the Gas Phase, Solution, and Protein Environments

Valentin Gogonea,*,†,‡ Jacinto M. Shy, II,† and Pradip K. Biswas†

Department of Chemistry, Cleveland State University, Cleveland, Ohio 44115, and Department of Immunology, Lerner Research Institute, Cleveland Clinic Foundation, Cleveland, Ohio 44195

Received: March 16, 2006; In Final Form: August 16, 2006

(6*R*)-5,6,7,8-Tetrahydrobiopterin (BH_4) is a key cofactor involved in the electron transfer to the P_{450} heme of nitric oxide synthase. We calculated the electronic structure of the neutral, cationic, and anionic forms of BH_4 in the gas phase, in solution (both dielectric and explicit water), and in the protein environment using density functional theory (B3LYP/6-31+G(d,p)). Subsequently, we derived the ionization potential (IP) and electron affinity (EA) of the cofactor in these chemical environments. We found that the electronic structure of BH_4 is susceptible to the presence of an external electric field and that conformational changes in the structure of BH_4 alone do not affect its electronic structure significantly. In the gas phase, water, and protein environments neutral BH_4 is the most stable species, while in the dielectric environment the anion becomes the most stable species. The IP of BH_4 in the protein environment is about half of that in the gas phase, and its EA is about 5 times smaller than that in the gas phase. Our results indicate that changes in the external electric field created by moving charged amino acid residues around BH_4 may lead to configurations that have the BH_4 ion as stable as or more stable than the neutral form, thus facilitating the electron transfer.

Introduction

(6*R*)-5,6,7,8-Tetrahydrobiopterin (BH_4) is a cofactor for several enzymes and can generate or scavenge reactive oxygen species.[1] Molecules that are related to biopterin include pterins, lumazines, alloxazines, folates, and riboflavins. The common structural feature of this group of molecules is a core of two or three fused heterocyclic six-membered rings. Pterins are very reactive; they form chelates (five-membered rings) with metals through the O^4 and N^5 atoms (see Scheme 1 for atom labeling). In BH_4 the pyrazine ring is hydrogenated, thus adding four more hydrogen atoms, two of which are bound to the two nitrogen atoms of this ring. The pK_a of N^5 is 5.6.[2] In solution, BH_4 can react with O_2,[3] hydrogen peroxide,[2,4] and peroxynitrite.[5] Glutathione, ascorbic acid, and dihydropteridine reductase (DHPR) reduce the quininoid form of BH_4,[6,7] and dihydrofolate reductase (DHFR) reduces the dihydro form (BH_2).[8] It has been suggested that the auto-oxidation proceeds through a radical species, which involves the N^5 atom.[2] The substitution of the hydrogen atom bound to N^5 with a methyl group[9] or the replacement of N^5 with a methylene bridge[10] in BH_4 decreases the susceptibility to auto-oxidation. Electronic structure calculations on BH_4 in the gas phase show that C^{4a} has maximum electron density and that the adjacent N^5 enhances the reactivity of C^{4a}.[1] The reduced susceptibility to oxidation of N^5-alkylated BH_4 was postulated to originate from the capability of the 5-methyl substituent to block the access of O_2 to the C^{4a} atom.[10]

Tetrahydrobiopterin has redox functions in aromatic amino acid hydroxylase (AAH)[11−13] and nitric oxide synthase (NOS).[14,15] In the latter it binds close to the P_{450} heme of NOS and is implicated in the timely transfer of one electron to the heme in the first step of arginine oxidation to *N*-hydroxyarginine by NOS. This paper presents such electronic properties of BH_4 such as the ionization potential (IP) and electron affinity (EA) calculated in the gas phase, solution, and protein environments, casting light on the possible scenarios of electron transfer from BH_4 to the P_{450} heme of NOS.

SCHEME 1

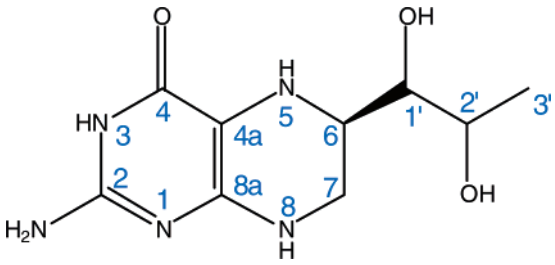

Theoretical Calculations

Quantum Mechanical Calculations. The optimized geometry and vibrational frequencies of neutral, cationic, and anionic

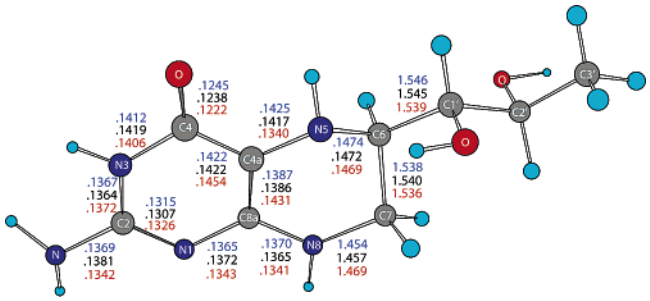

Figure 1. Bond lengths (nm) in neutral (black), cationic (red), and anionic (blue) BH_4. The geometries have been optimized in the gas phase using density functional theory (B3LYP/6-31+G(d)).

* Author to whom correspondence should be addressed. E-mail: v.gogonea@csuohio.edu.
† Cleveland State University.
‡ Cleveland Clinic Foundation.

10.1021/jp061653q CCC: $33.50
Published on Web 10/20/2006

TABLE 1: Comparison between the X-ray Crystal Structure of Tetrahydrobiopterin Bound to Nitric Oxide Synthase and the Structure Calculated by Density Functional Theory and Molecular Mechanics (with the OPLS Force Field)

internal coordinate	geometry				
	QM[a]	crystal[b]	Δ_{QM-C}[c]	MM[d]	Δ_{QM-MM}[e]
			Bond Length[f]		
N^1-C^2	0.1307	0.1346	−0.0039	0.1322	−0.0015
N^1-C^{8a}	0.1372	0.1371	0.0001	0.1389	−0.0017
C^2-N^3	0.1364	0.1352	0.0012	0.1349	0.0015
N^3-C^4	0.1419	0.1402	0.0017	0.1403	0.0016
C^4-C^{4a}	0.1422	0.1417	0.0005	0.1420	0.0002
$C^{4A}-N^5$	0.1417	0.1448	−0.0031	0.1408	0.0009
$C^{8A}-N^8$	0.1365	0.1333	0.0032	0.1382	−0.0017
N^5-H	0.1019			0.1023	−0.0004
N^5-C^6	0.1472	0.1514	−0.0042	0.1480	−0.0008
C^6-C^7	0.1540	0.1509	0.0031	0.1556	−0.0016
C^7-N^8	0.1457	0.1455	0.0002	0.1468	−0.0011
N^8-H	0.1009			0.1013	−0.0004
RMSD[g]			0.0026		0.0012
MAX[h]			0.0042		0.0017
			Bond Angle[i]		
$C^4-C^{4a}-N^5$	119.4	117.6	1.8	118.5	0.9
$C^{4a}-N^5-C^6$	115.5	111.0	4.5	116.0	−0.5
$C^{4A}-N^5-H$	108.9			110.1	−1.2
C^6-N^5-H	113.9			113.6	0.3
$N^5-C^6-C^7$	108.6	108.9	−0.3	107.7	0.9
$C^6-C^7-N^8$	110.5	111.7	−1.2	109.9	0.6
$C^{8a}-N^8-C^7$	120.7	119.9	0.8	119.8	0.9
$C^{8a}-N^8-H$	116.5			117.2	−0.7
C^7-N^8-H	120.9			120.3	0.6
RMSD			2.4		0.9
MAX			4.5		1.2
			Dihedral Angle[i]		
$C^4-C^{4a}-N^5-H$	−25.3			−22.4	−2.9
$N^1-C^{8a}-N^8-H$	−7.3			−9.7	2.4
$N^5-C^{4a}-C^{8a}-N^8$	−3.4	−1.9	1.3	−1.1	2.2
$C^{8a}-C^{4a}-N^5-C^6$	24.9	29.0	−4.1	23.1	1.8
$C^{4a}-C^{8a}-N^8-C^7$	10.7	1.6	9.1	9.7	1.0
$C^{4a}-C^{8a}-N^8-H$	175.1			171.4	3.7
$C^{4a}-N^5-C^6-C^7$	−49.0	−53.8	4.8	−48.8	−0.2
$C^{4a}-N^5-C^6-H$	70.7			69.5	1.2
$N^5-C^6-C^7-N^8$	53.6	53.8	−0.2	54.5	−0.9
$C^6-C^7-N^8-C^{8a}$	−36.1	−28.6	−7.5	−37.1	1.0
$C^6-C^7-N^8-H$	160.0			161.9	−1.9
RMSD			3.9		4.3
					3.2[j]
MAX			9.1		10.2
					6.4[j]

[a] The structure of BH_4 obtained by calculation using density functional theory (B3LYP/6-31+G(d,p)) with the Gaussian 98 program.[26] [b] The structure of BH_4 used in this comparison was extracted from the crystal structure of iNOSoxy dimer (1NSI).[34] [c] Difference between the same internal coordinate measured in the quantum mechanically calculated (density functional theory) structure and the crystal structure of BH_4. [d] The structure of BH_4 calculated with the molecular mechanics program Gromacs [31] using the OPLS force field[40] derived by the GA method. [e] Difference between the same internal coordinate measured in the density funtional theory structure and the molecular mechanics optimized structure of BH_4. [f] Given in units of nm. [g] Root-mean-square deviation for all bond lengths in BH_4. [h] Maximum difference. [i] Given in units of deg. [j] Calculated without considering the dihedral angles that contain at least one hydrogen atom.

forms of BH_4 have been calculated by quantum mechanics using the density functional theory (B3LYP Hamiltonian with Becke3 exchange[16] and Lee−Yang−Parr correlation[17] functionals) with the 6-31+G(d,p) basis set. Single-point calculations have also been performed with Møller−Plesset second-order perturbation theory (MP2)[18−23] with the 6-31+G(d,p) basis set and the B3LYP hybrid method using the 6-311+G(d,p) and 6-311++G-(d,p) basis sets. The electrostatic potential (ESP)-derived charges for atoms in neutral BH_4 (used in deriving OPLS parameters[24]) were obtained from the wave function of the optimized geometry

TABLE 2: Bond and Dihedral Angles in the Optimized Gas-Phase Geometries[a] of the Neutral, Cationic, and Anionic Forms of Tertrahydrobiopterin

	neutral	cation	N−C[b]	anion	N−A[c]
			Bond Angle[d]		
$N^1-C^{8a}-C^{4a}$	123.7	122.6	1.1	124.2	−0.5
$C^4-C^{4a}-C^{8a}$	119.3	119.4	0.1	119.2	0.1
$C^{4a}-C^{8a}-N^8$	119.6	117.8	1.8	119.4	0.2
$N^5-C^{4a}-C^{8a}$	120.8	121.3	−0.5	121.6	−0.8
$C^{4a}-N^5-C^6$	113.8	122.0	−8.2	115.0	−1.2
$N^5-C^6-C^7$	108.4	108.7	−0.3	108.6	−0.2
$N^5-C^6-C^{1'}$	106.6	109.2	−2.6	106.4	0.2
$C^6-C^7-N^8$	110.8	110.4	0.4	110.4	0.4
$C^7-N^8-C^{8a}$	122.3	121.8	0.5	121.0	1.3
			Dihedral Angle[d]		
$C^4-C^{4a}-N^5-C^6$	−148.4	−170.8	22.4	−153.6	5.2
$C^{4a}-N^5-C^6-C^7$	−53.9	−34.7	−19.2	−48.6	−5.3
$C^{4a}-C^{8a}-N^8-C^7$	0.3	12.9	−12.6	10.8	−10.5
$C^{4a}-N^5-C^6-C^{1'}$	−175.8	−159.0	−16.8	−170.3	−5.5
$N^5-C^6-C^7-N^8$	50.6	47.0	3.6	53.5	−2.9
$C^6-C^7-N^8-C^{8a}$	−25.7	−39.8	14.1	−36.4	10.7

[a] Calculated at B3LYP/6-31+G(d,p) level of density functional theory. [b] Neutral − cation. [c] Neutral − anion. [d] Given in units of deg.

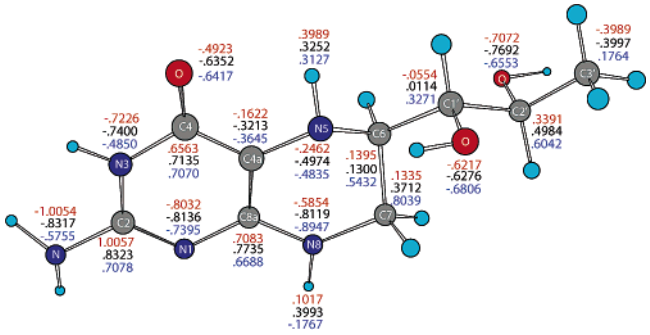

Figure 2. Merz−Kollman ESP-derived partial atomic charges for atoms in neutral (black), cationic (red), and anionic (blue) BH_4 calculated by density functional theory (B3LYP/6-31+G(d)) in the gas phase.

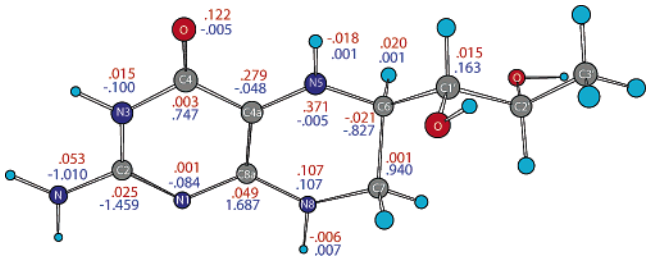

Figure 3. Spin densities for cationic (red) and anionic (blue) BH_4 calculated by density functional theory (B3LYP/6-31+G(d)) in the gas phase.

using the Merz−Kollman[25] method as implemented in the Gaussian 98 program.[26] The IP and EA of BH_4 in the gas phase, dielectric[27] and explicit water (TIP4P[28]), and protein environments (NOS) were calculated at the B3LYP/6-31+G(d,p) level. Graphical representations of the highest occupied molecular orbital (HOMO), singly occupied molecular orbital (SOMO), and lowest unoccupied molecular orbital (LUMO) data in CUBE files, in addition to spin densities, were created using the VMD program[29] and the POV−Ray visualization program.[30]

Force Field Parametrization. To perform energy minimization of BH_4 in water and protein environments (NOS) we have developed OPLS parameters[24] for the following species: neutral BH_4, P_{450} heme, and the $[Zn(cysteine)_4]^{2-}$ complex. The

TABLE 3: Root-Mean-Square Deviation (RMSD) of Vibrational Frequencies for Tetrahydrobiopterin, Dioxy−Iron Porphirin Methylthiolate Complex, Tetramethylthiolate−Zinc Complex, Glycine, and Tyrosine

compound[a]	RMSD[b]
BH_4	38
O_2−Fe−PP−SMe[c]	43
$[Zn(MeS)_4]^{2-}$ [d]	50
glycine	94
tyrosine	65

[a] The vibrational modes were calculated with the OPLS force field obtained by the GA method and implemented in Gromacs program.[31] [b] Root-mean-square deviations are given in units of in cm^{-1}. [c] Dioxy−iron porphyrin methylthiolate complex. [d] Tetramethylthiolate−Zn complex.

TABLE 4: Root-Mean-Square Deviation (RMSD) between the Quantum Mechanical and the Molecular Mechanical Optimized Structures of Tetrahydrobiopterin, Dioxy−Iron Porphirin Methylthiolate Complex, and Tetramethylthiolate−Zinc Complex

	RMSD[a]		
compound	bond length (nm)	bond angle (deg)	dihedral angle (deg)
BH_4	0.0013	0.89	20.6
	0.0012	1.57	15.0
O_2−Fe−PP−SMe[b]	0.0010	0.98	2.15
	0.0010	0.98	2.15
$[Zn(MeS)_4]^{2-}$ [c]	0.0036	4.62	23.20
	0.0036	4.62	23.20

[a] First row: RMSD for parametrized bond lengths, bond angles and dihedral angles; second row: total RMSD. [b] Dioxy−iron porphyrin methylthiolate complex. [c] Tetramethylthiolate−Zn complex.

molecular mechanics optimized geometry and vibrational frequencies of neutral BH_4, methylthiolate dioxy−iron (Fe^{2+}) porphyrin complex, and the tetramethylthiolate−zinc complex $[Zn(MeS)_4]^{2-}$ were calculated using the OPLS force field[24] as implemented in the molecular dynamics simulation program Gromacs.[31] The OPLS force field parameters used for atom types of BH_4, P_{450} heme, and $[Zn(cysteine)_4]^{2-}$ complex have been derived in the following way: (a) OPLS atom types similar to those found in these species were first identified and assigned estimated parameters; (b) the geometrical parameters (equilibrium bond lengths, bond angles, Ryckaert−Bellemans coefficients,[32] and improper dihedral angles) were adjusted using a genetic algorithm (GA) optimization program[33] such that the root-mean-square deviation (RMSD) in the internal coordinates of the quantum and molecular mechanics calculated structures is minimum; (c) the OPLS force constants for bond stretching and angle bending were adjusted (using the GA) such that the RMSDs between the vibrational frequencies of BH_4, methylthiolate dioxy-iron (Fe^{2+}) porphyrin, and the tetramethyltiolate−zinc complexes calculated by quantum mechanics and molecular mechanics methods were less than the RMSDs calculated for a few amino acids with OPLS parameters (defined in the OPLS force field implemented in the Gromacs program[31]).

Molecular Mechanics Calculations. The Protein Data Bank (PDB) structure 1NSI[34] was used to obtain an energy-minimized structure of the solvated iNOSoxy dimer. The structure was prepared as follows: (a) One oxygen molecule was bound to Fe^{2+} of heme of each monomer by modifying the PDB file (the first electron transfer reduces Fe^{3+} to Fe^{2+}, which allows oxygen to bind to the iron ion, and the second electron transfer is facilitated by BH_4); (b) hydrogen atoms were added, and protonation states were assigned (corresponding to pH = 7) using the Gromacs utility pdb2gmx. In this particular configuration of 1NSI, there are three charged amino acids within 0.5 nm of BH_4 (chain A): Arg^{199A}, Arg^{381A}, and Glu^{479B}. It seems that among these charged amino acid residues only Arg^{381A} interacts significantly with BH_4. (Arg^{381A} makes a hydrogen bond (0.205 nm) with O^4 of BH_4, which is 0.242 nm in the

TABLE 5: Ionization Potential and Electron Affinity[a] of (6*R*)-5,6,7,8-Tetrahydrobiopterin in Gas Phase, Dielectric, Water, and Protein Environments

	energy[b]				
environment	neutral	cation	anion	IP[c]	EA[c]
gas phase	−851.509486	−851.285676	−851.495086	6.09	−0.39
	−851.7029332[d]	−851.4540438	−851.6868365	6.77	−0.44
	−851.7033758[e]	−851.4545306	−851.6993969	6.77	−0.11
	−849.083620[f]	−848.825127	−849.011603	7.09	−1.96
	−851.467803[g]	−851.225248	−851.452508	6.60	−0.42
	−851.475396[h]	−851.241385	−851.459583	6.37	−0.43
	−851.478942[i]	−851.241096	−851.4626326	6.47	−0.44
water[j]	−1195.536599	−1195.2724002	−1195.523429	7.19	−0.36
dielectric[k]	−851.556900	−851.379800	−851.587815	4.82	0.84
protein[l]	−12441.231311	−12441.072356	−12441.139355	4.33	−2.50
	−12441.221713	−12441.096451	−12441.099584	3.41	−3.32

[a] Calculations performed by density functional theory at B3LYP/6-31+G(d,p) level unless otherwise specified. All calculations were performed with the Gaussian 98 program.[26] [b] Given in units of hartree. [c] Given in units of eV. [d] B3LYP/6-311+G(d,p) level. [e] B3LYP/6-311++G(d,p) level. [f] MP2/6-31+G(d,p) level. [g] Calculation on the optimized geometry of BH_4 in solution without the external electric field generated by the surrounding water. [h] Calculation on the optimized geometry of BH_4 in the protein environment (chain A of the iNOSoxy dimer) without the external electric field generated by the surrounding amino acids, water molecules, and P_{450} heme. [i] Calculation on the optimized geometry of BH_4 in the protein environment (chain B of the iNOSoxy dimer) without the external electric field generated by the surrounding amino acids, water molecules, and P_{450} heme. [j] Calculation on the optimized solution geometry of BH_4 with the external electric field generated by point charges representing TIP4P water molecules. The cofactor's molecular mechanics force field is described by OPLS parameters[24] obtained as described in the Theoretical Calculations section. The optimization was performed on BH_4 immersed in a box of 603 water (TIP4P) molecules. [k] Calculation on the gas-phase optimized geometry of BH_4 with the external electric field generated by a polarizable dielectric (dielectric constant = 80). [l] Calculation on the optimized geometry of BH_4 in the protein environment (iNOSoxy) with the external electric field generated by the point charges representing surrounding amino acids, water molecules, and P_{450} heme. The molecular mechanics force fields for BH_4, P_{450} heme, and $[Zn(Cys)_4]^{2-}$ complex are described by OPLS parameters [24] obtained as described in the Theoretical Calculations section. The optimization was performed on the iNOSoxy dimer immersed in a box of 19 529 water molecules (TIP4P) and 8 counterions (Na^+). First row, data for BH_4 bound at chain A of the iNoxy dimer; second row, data for BH_4 bound to chain B.

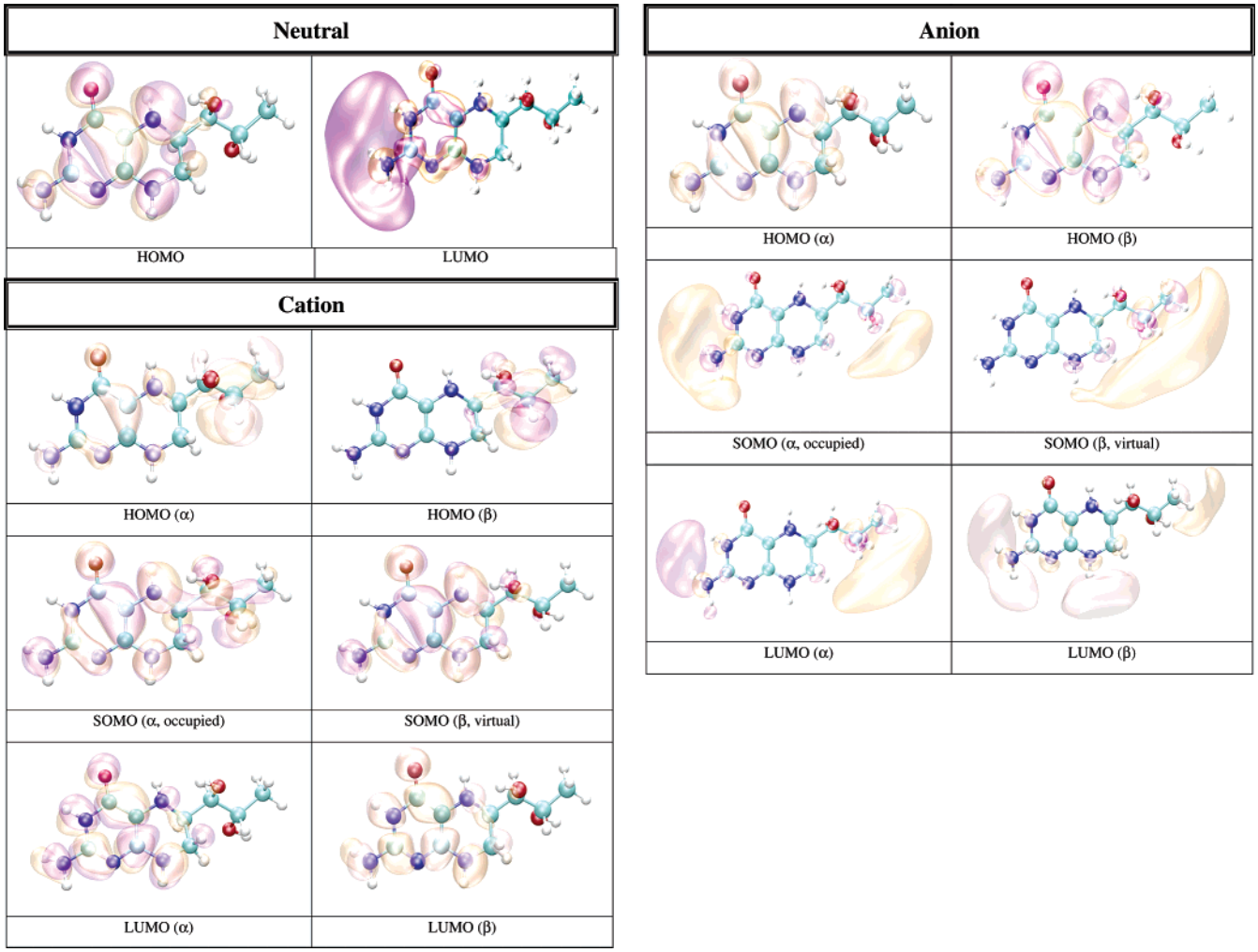

Figure 4. HOMO and LUMO for neutral (N) BH_4; HOMO SOMO, and LUMO for the BH_4 cation (C) and anion (A) calculated by density functional theory (B3LYP/6-31+G(d)) in the gas phase with Gaussian 98. The molecular orbital pictures were obtained from CUBE Gaussian 98 files and displayed with the VMD and POV−Ray programs.

crystal structure.) Because the crystal structure (1NSI) indicates that the C−NH_2 bonds of the guanidinium moiety of Arg^{381A} are equal, we considered Arg^{381} (in both monomers) to be protonated (charge +1 e.u.). Following the same argument we also considered Arg^{199} to be protonated. Note that this residue together with Trp^{463} and BH_4 stack on top of each other like a sandwich (with Trp^{463} between the other two), and it is reasonable to believe that the positive charge of Arg^{199}, which is delocalized on the guanidinium moiety, involves this residue in a π-stacking interaction between Trp^{463} and BH_4. The residue Glu^{479B}, which is 0.466 nm (0.545 nm in the crystal structure) from the hydroxy tail of BH_4 (docked in chain A), does not interact with the cofactor and was considered to be deprotonated. There is no experimental evidence that these residues should have a different protonation state than the one assigned in this study. (c) The iNOSoxy structure was solvated in a box of 19 529 water molecules (TIP4P); (d) eight Na^+ ions were added at random positions in the solvent to neutralize the negative charge of the dimer. The potential energy of the solvated iNOSoxy was minimized using the OPLS force field[24] implemented in Gromacs.[31]

Results and Discussion

Geometry and the Electronic Structure of Neutral, Cationic, and Anionic BH_4. *Geometry.* Figure 1 shows the quantum mechanically optimized geometry of BH_4. This figure also displays a comparison between the bond lengths of the neutral (black), cationic (red), and anionic (blue) forms of BH_4 in the pyrimidine (aromatic) and tetrahydropyrazine rings. One interesting structural detail of neutral BH_4 is the nonequivalence of the N^5 and N^8 nitrogen atoms (Scheme 1). The atom N^5 is hybridized sp^3 (the $C^{4a}-N^5$ bond length is 0.1417 nm, the $C^{4a}-N^5-H$ bond angle is 108.9°, and the $C^4-C^{4a}-N^5-H$ dihedral angle is −25.3°), while atom N^8 is hybridized sp^2 (the $C^{8a}-N^8$ bond length is 0.1365 nm, the $C^{8a}-N^8-H$ bond angle is 116.5°, and the $N^1-C^{8a}-N^8-H$ dihedral angle is −7.3°). This structural aspect is important because it was hypothesized that in the BH_4 cation the spin density of the unpaired electron is mainly localized at N^5.[35] Table 1 shows that the geometry of neutral BH_4 calculated at the B3LYP/6-31+G(d,p) level is in good agreement with the structure of BH_4 (without H atoms) bound to chain A of the iNOSoxy (PDB code 1NSI) dimer. The RMSD of the bond lengths given in Table 1 is 0.0026 nm, and the RMSDs for the bond and dihedral angles are 2.4° and 3.9°, respectively. Figure 1 shows one noticeable aspect of the difference in structure between the neutral, cationic, and anionic forms of BH_4. The alternation of bond lengths involving the C^{4a}, C^{8a}, and N^5 atoms is reversed in the cation as compared with the neutral and anionic BH_4: $C^{4a}-N^5$ is 0.1417 nm in the neutral form and 0.1425 nm in anionic form versus 0.1340 nm in the cation, while $C^{4a}-C^{8a}$ is 0.1386 nm in the neutral form and 0.1387 nm in the anionic form versus 0.1431 nm in the

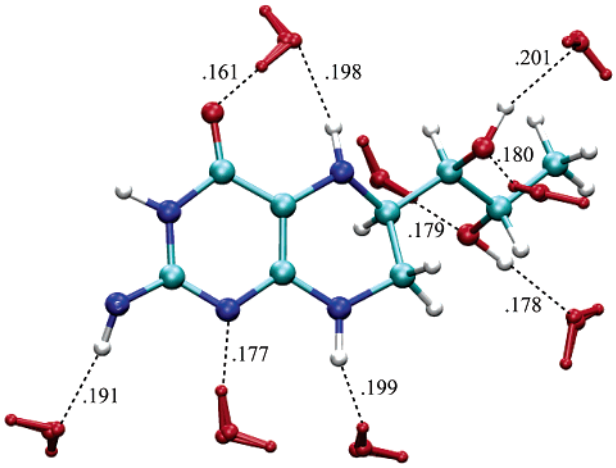

Figure 5. Water configuration (red) around neutral BH_4. The water (TIP4P) box containing one molecule of BH_4 (OPLS) was energy-minimized using the Gromacs program. There are nine hydrogen bonds (black dashed lines) between BH_4 and water within 0.2 nm.

cation. Table 2 shows a comparison of a subset of bond and dihedral angles (mostly defining the pyrimidine and tetrahydropyrazine rings). As in the case of bond lengths, a substantial change in the bond angle (8.2°) is observed between the cationic and neutral BH_4 and involves the N^5 atom (e.g., the $C^{4a}-N^5-C^6$ angle is 113.8° (neutral), 115.0° (anion), and 122.0° (cation)). Overall, the anion geometry is closer to the geometry of neutral BH_4 than the cation geometry. This may be one of the reasons that the EA of BH_4 in the gas phase is less than 1 eV, while the IP is approximately 6 eV (vide infra).

Charges and Spin Density. ESP-derived charges have been calculated using the ChelpG[36] and Merz−Kollman (MK)[25] methods as implemented in the Gaussian 98 program.[26] The ChelpG-derived charges (not shown) are slightly smaller than the MK-derived charges in the pyrimidine ring of BH_4 but are larger in the tetrahydropyrazine ring of BH_4. The partial charge of N^5 (ChelpG, −0.4974 e.u.; MK, −0.4958 e.u.) is about half the partial charge of N^8 (ChelpG, −0.8119 e.u.; MK, −0.8089 e.u.). Figure 2 shows MK charges for the neutral (black), cationic (red), and anionic (blue) forms of BH_4. The C^{4a}, N^5, and N^8 atoms are negatively charged (−0.3213, −0.4974, and −0.8119 e.u., respectively) in neutral BH_4. Removing one electron from BH_4 makes these atoms less negative (−0.1622, −0.2462, and −0.5854 e.u., respectively), but adding one electron causes a small change in the partial charges of these atoms (−0.3645, −0.4835, and −0.8947 e.u., respectively). However, the partial charges on the C^6 and C^7 atoms (in neutral BH_4 0.1300 and 0.3712 e.u., respectively) affect the anion more (0.5432 and 0.8039 e.u., respectively) than the cation (0.1395 and 0.1335 e.u., respectively). It should be noted that the charge of the N^3 atom is less negative in the anion (−0.4850 e.u.) compared to the neutral and cationic forms (−0.7400 and

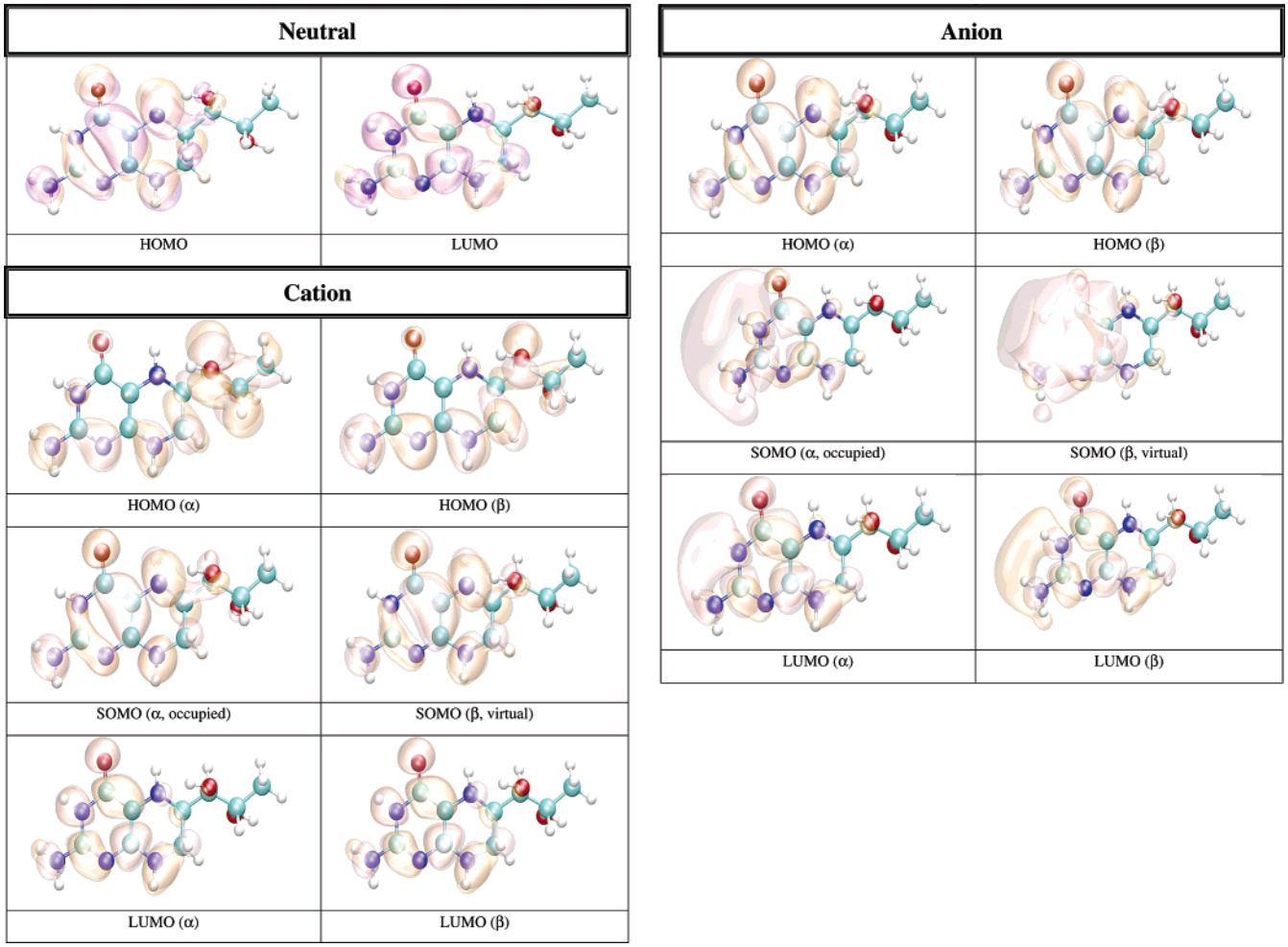

Figure 6. HOMO and LUMO for neutral (N) BH_4; HOMO SOMO, and LUMO for the BH_4 cation (C) and anion (A) calculated by density functional theory (B3LYP/6-31+G(d)) in dielectric (dielectric constant 80.0) with Gaussian 98. The molecular orbital pictures were obtained from CUBE Gaussian 98 files and displayed with the VMD and POV−Ray programs.

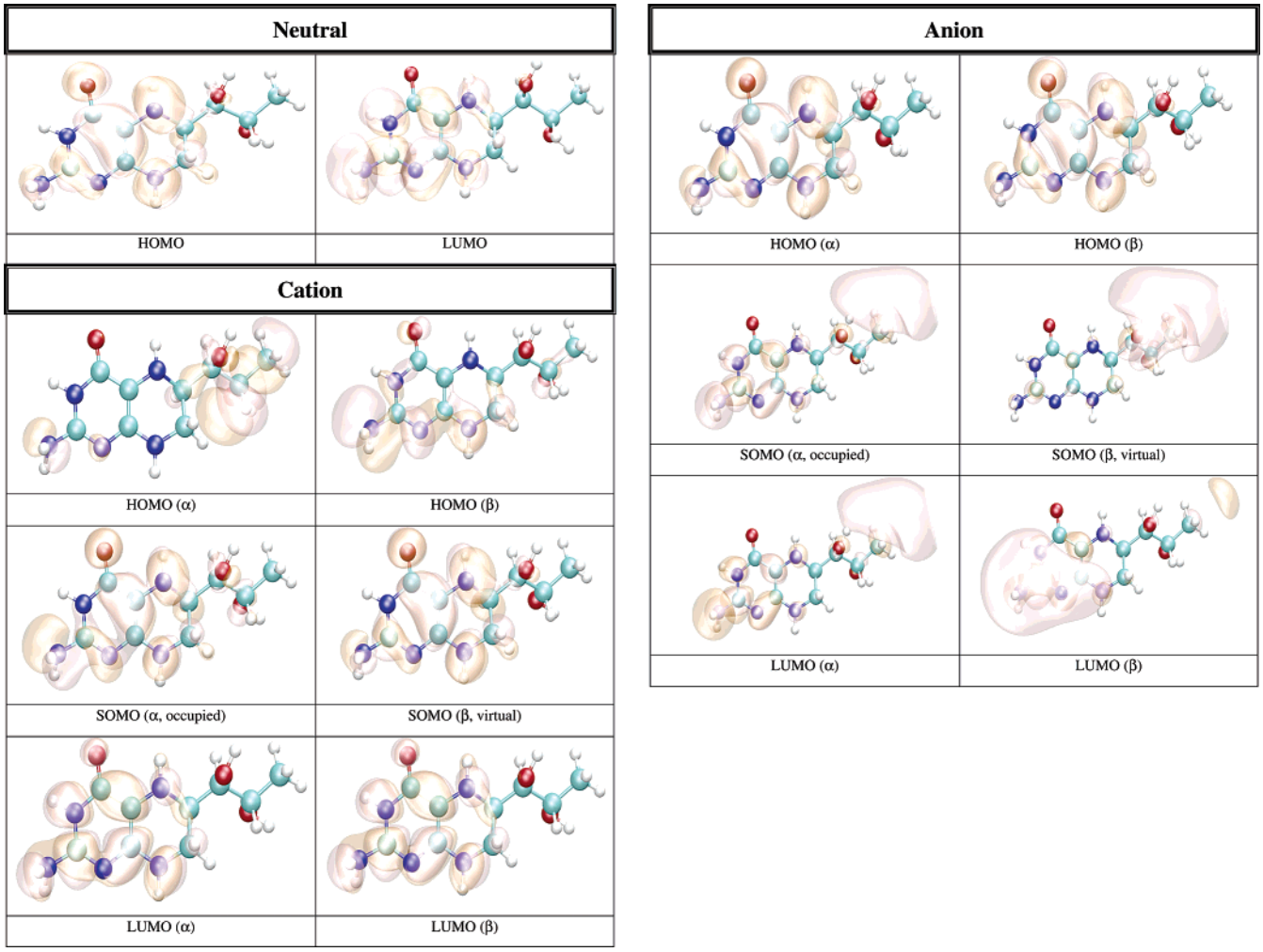

Figure 7. HOMO and LUMO for neutral (N) BH_4; HOMO, SOMO, and LUMO for the BH_4 cation (C) and anion (A) calculated by density functional theory (B3LYP/6-31+G(d)) in water (TIP4P) with Gaussian 98. The molecular orbital pictures were obtained from CUBE Gaussian 98 files and displayed with the VMD and POV−Ray programs.

−0.7226 e.u., respectively). The SOMO of the anion is mostly localized on the side of the pyrimidine ring containing the N^3 atom and NH_2 group (vide infra), whereas the virtual SOMO is mostly localized near the hydroxy tail of BH_4. Figure 3 gives the spin densities for the cation (red) and anion (blue). In the case of the cation, more than half of the spin density is localized on the C^{4a} and N^5 atoms, which supports an earlier suggestion that much of the spin density is localized on atom N^5. The results for the anion are more difficult to rationalize since the spin densities oscillate from positive to negative values. However, a graphical representation of the spin density for the anion (vide infra) indicates that it is mostly localized on the side of the pyrimidine ring containing the N^3 atom and the NH_2 group.

OPLS Force Field for BH_4, P_{450} Heme, and the $Zn(Cys)_4$ Complex. The quality of the OPLS force field parameters (for BH_4 atom types) was assessed by comparing the optimized geometry of BH_4, calculated by quantum mechanics and molecular mechanics methods, and the geometry of BH_4, extracted from the crystal structure of the oxygenase domain from inducible nitric oxide synthase (iNOSoxy, PDB code 1NSI). The discussion here will be focused on the geometry of the pyrimidine and tetrahydropyrazine rings of BH_4. Table 1 shows the comparison of the quantum mechanical, molecular mechanical, and crystal structures using a subset of the internal coordinates of the atoms that compose these two rings. The difference between the quantum mechanical structure, on one hand, and the crystal and molecular mechanical structures, on the other hand, are expressed as RMSDs for bond lengths, bond angles, and dihedral angles, respectively. The RMSD between the QM and the MM structures (QM−MM) for the bond lengths is 0.0012 nm. For the bond angles the QM−MM is 0.9°, and for dihedral angles the QM−MM RMSD is 4.3°. The QM−MM RMSD decreases to 3.2° when the dihedral angles that include hydrogen atoms are excluded. (The crystal structure has no hydrogen atoms.) Table 1 shows that the MM-optimized geometry is very close to the QM-optimized and crystal structure geometries.

To produce realistic molecular dynamics (MD) simulations it is essential that the derived force field parameters correctly reproduce not only the equilibrium geometry but also the dynamics of the molecule (i.e., the normal modes of vibration). The OPLS parameters that modulate the MM-calculated vibrational frequencies are the force constants for bond stretching, angle bending, and dihedral angle torsion. By comparing the QM- and MM-derived vibrational frequencies we assess the quality of these force constants. The RMSD of 90 normal modes of vibration for BH_4 is 38 cm^{-1} with the largest difference being 131 cm^{-1} for normal mode 75 (Supporting Information). Table 3 gives a comparison between the QM−MM RMSDs of vibrational frequencies calculated for BH_4, glycine (94 cm^{-1}), and tyrosine. (65 cm^{-1}). Table 3 shows that the force field derived in this work for BH_4 is of better quality than the average

OPLS parameters used for amino acids. In addition to the BH_4 cofactor, the iNOSoxy dimer contains a P_{450} heme cofactor and a Zn−cysteine bridge between the two monomers.[37] To perform an energy minimization of the iNOSoxy dimer in water we derived OPLS parameters for the P_{450} heme cofactor[33] and a $[Zn(Cys)_4]^{2-}$ complex.[38] Tables 3 and 4 list the RMSDs for geometrical parameters (Table 4) as well as for vibrational frequencies (Table 3) for these two moieties.

IP and EA of BH_4 in the Gas Phase, Solution, and Protein Environments. The IP and EA of BH_4 in different chemical environments (e.g., vacuum, solution, protein environment) are probably the most relevant electronic properties for understanding the involvement of BH_4 in the electron transfer in NOS because, unlike in other enzymes, the cofactor in NOS is oxidized/reduced without changing protonation states.[1] Calculations show that the wave function of BH_4 is highly polarizable and an external electric field shifts the frontier molecular orbitals (i.e., the HOMO, LUMO, and SOMO for the cation and anion) and thus changes the IP and EA of BH_4. We calculated the IP and EA of BH_4 in the gas phase, dielectric[27] (dielectric constant 80.0) and explicit water (TIP4P[28]), and protein environments (iNOSoxy) using density functional theory at the B3LYP/6-31+G(d,p) level.

Gas Phase. In the gas phase neutral BH_4 is more stable than both its cation and anion. Because there are fewer geometrical differences between the anionic and the neutral BH_4 than between the cationic and neutral BH_4 (vide supra), one expects that the difference in energy between the anionic and the neutral BH_4 to be smaller than the difference between the cationic and the neutral BH_4. Table 5 lists the IPs and EAs of BH_4 calculated in different chemical environments. The IP increases with the use of more sophisticated basis sets, e.g., from 6.09 eV (6-31+G(d,p)) to 6.77 eV (6-311+G(d,p) and 6-311++G(d,p)). The EA, however, does not show a definite trend, e.g., −0.39 eV (6-31+G(d,p)), −0.44 eV (6-311+G(d,p)), −0.11 eV (6-311++G(d,p)). MP2 calculations performed on BH_4 using the 6-31+G(d,p) basis set yield 7.09 eV for the IP and −1.96 eV for the EA of BH_4. It is worthy of note that the IP and EA change only slightly with a change in the conformation of BH_4 and that they are mostly susceptible to the action of an external electric field. Thus, when the calculation is performed on the geometry of BH_4 in solution or on the geometry of BH_4 in the protein environment without the external electric field due to point charges the IP and EA change from 6.09 and −0.39 eV in the gas phase, to 6.60 and −0.42 eV in water, to 6.37 and −0.43 eV for BH_4 bound to chain A and to 6.47 and −0.44 eV for BH_4 bound to chain B of the iNOSoxy dimer. Figure 4 shows graphical representations of the HOMO and LUMO for the neutral BH_4 and of the HOMO, SOMO, and LUMO of the BH_4 cation and anion. The pictures were obtained by visualizing CUBE files (obtained with Gaussian 98[26]) with the VMD[29] and POV−Ray[30] programs. Figure 4 shows that the HOMO of neutral BH_4 is localized on the two rings, while the LUMO is mostly localized near the pyrimidine ring (close to the N^3 atom and NH_2 group). The SOMO (occupied) of the anion is similar to the LUMO of the neutral BH_4 (localized mostly in the same region), though the virtual SOMO is mainly localized near the hydroxy tail of BH_4. The localization of the occupied SOMO of the anion confirms that the unpaired electron is basically unbound in the gas phase. (The EA is negative.) However, the occupied SOMO of the cation spreads over the entire molecule, whereas the virtual SOMO is mostly localized on the two rings of BH_4 and is very similar to the HOMO of the neutral BH_4. Another distinctive feature of these frontier orbitals is that the LUMO (for α and β electrons) of the cation are very different from the LUMO of the neutral species and SOMO of the anion (Figure 4). This observation is valid for all chemical environments of BH_4 used in this study (vide infra).

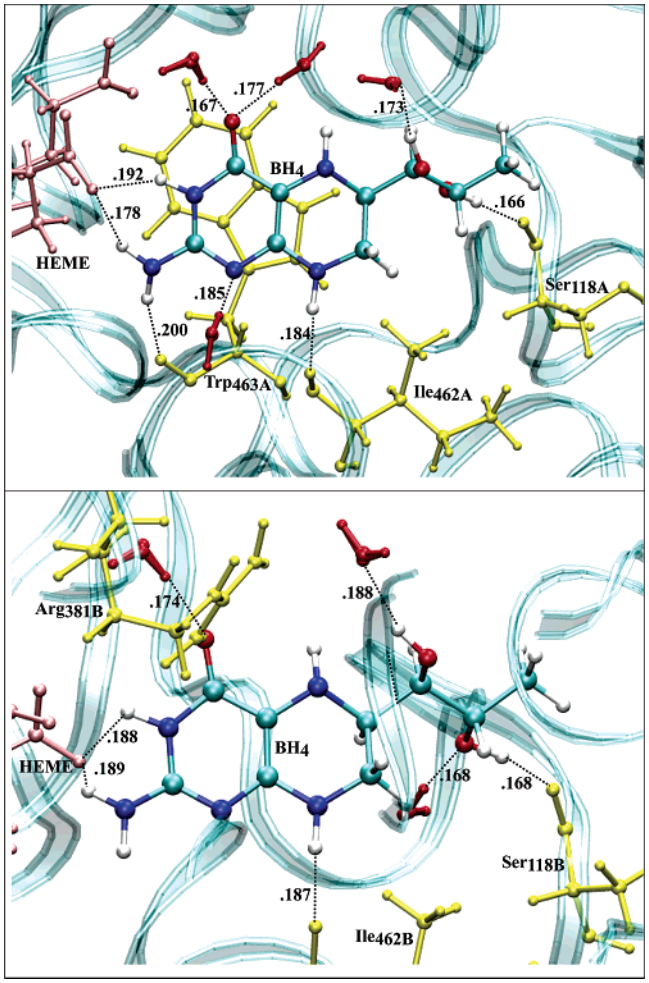

Figure 8. Amino acid residues (yellow), P_{450} heme (pink), and solvent (red) configuration around neutral BH_4 bound to chain A (top) and chain B (bottom) of the iNOSoxy dimer. The water (TIP4P) box containing a iNOSoxy dimer (OPLS) was energy-minimized using the Gromacs program. There are nine hydrogen bonds (black dashed lines) between BH_4 (chain A) and the amino acid residues, heme, and water within 0.2 nm and seven hydrogen bonds for BH_4 bound to chain B.

Solution. The IP and EA of BH_4 have been calculated both in dielectric and explicit water (TIP4P). The calculation in dielectric (dielectric constant 80.0) gives the effect of an average electric field on the IP and EA due to water polarization, and the calculation in explicit water introduces anisotropy in the electric field due to specific positions of water molecules and the presence of hydrogen bonds. The calculations on BH_4 in dielectric and explicit water show a substantial effect from the external electric field on the IP and EA of BH_4. Calculation in dielectric gives the average effect of water polarization on the electronic structure of BH_4. Thus the IP decreases to 4.82 eV, while the EA becomes positive (0.84 eV), which makes the anion more stable than neutral BH_4 in dielectric. This result suggests that one-electron reduction of BH_4 in water should be easy, while one-electron oxidation may not be easy.[39] The calculation in explicit water (Table 5) shows that the IP (7.19 eV) and EA (−0.36 eV) values are closer to the vacuum values rather than the dielectric values. Figure 5 shows that neutral BH_4 makes nine hydrogen bonds with surrounding water molecules (in this particular energy-minimized configuration).

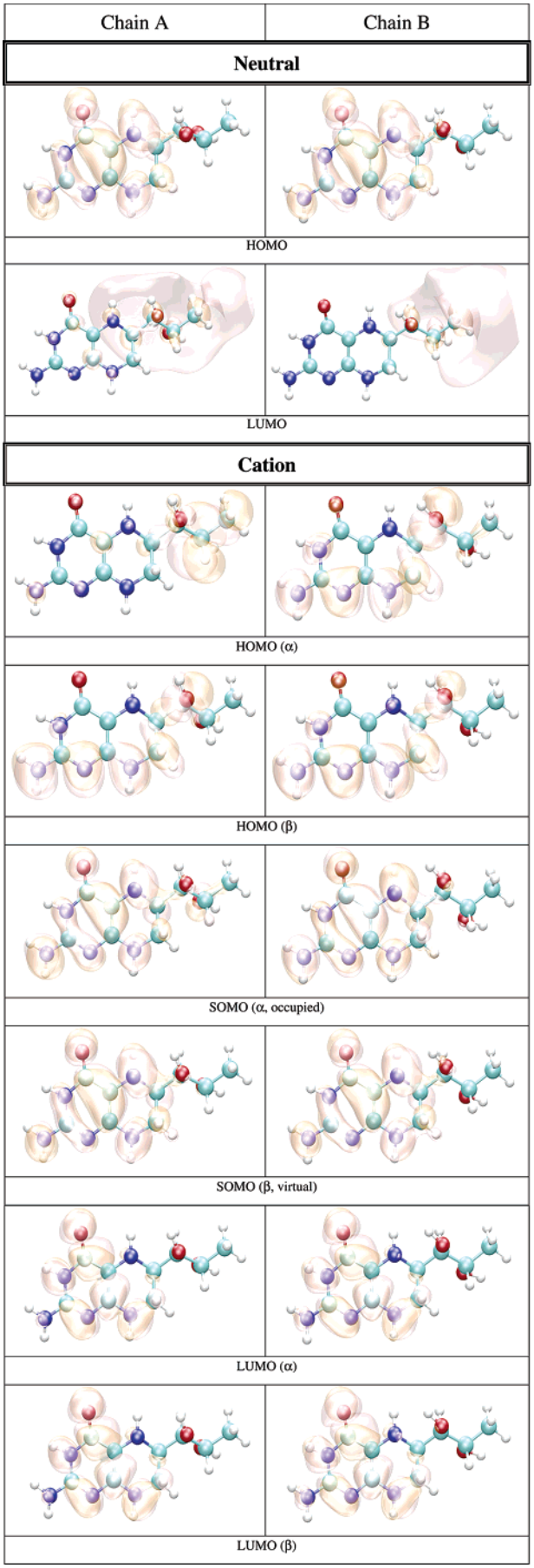

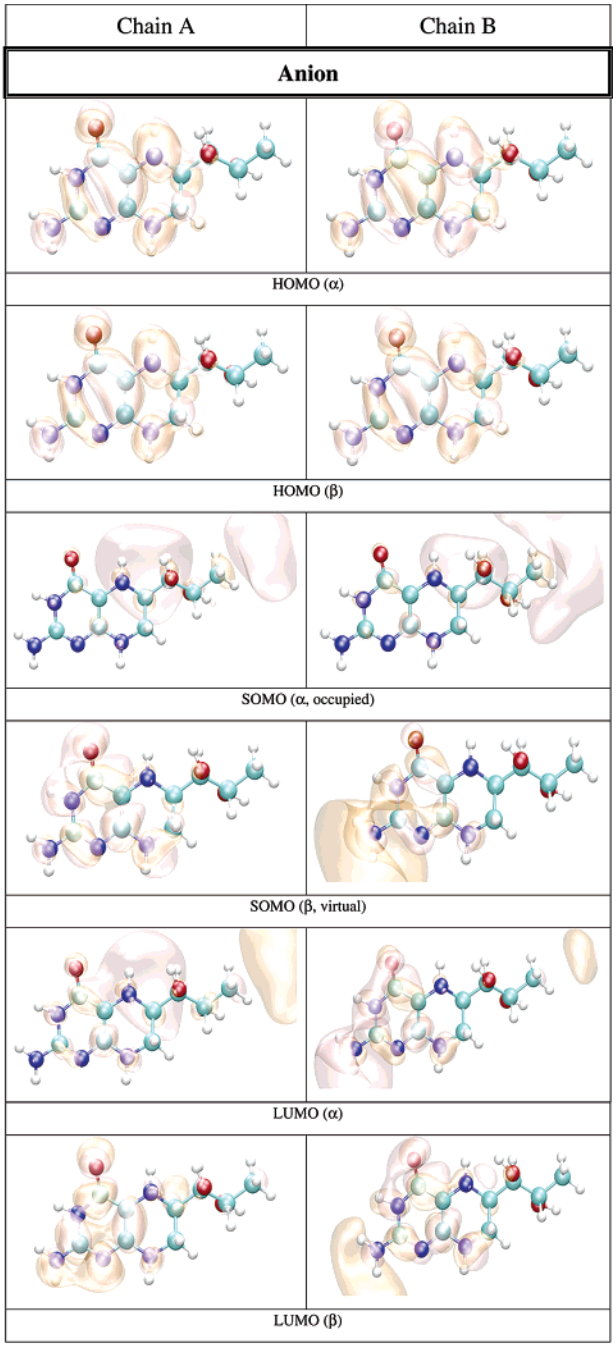

Figure 9. HOMO and LUMO for neutral (N) BH_4; HOMO, SOMO, and LUMO for the BH_4 cation (C) and anion (A) from both iNOSoxy monomers (chains A and B), calculated by density functional theory (B3LYP/6-31+G(d)) in the protein environment with Gaussian 98. The molecular orbital pictures were obtained from CUBE Gaussian 98 files and displayed with the VMD and POV−Ray programs.

Five of these hydrogen bonds are made with the BH_4 tail, while the remaining four hydrogen bonds are made with the NH_2 group, N^1, O,[4] H^5, and H^8 (Scheme 1). Figures 6 and 7 show pictures of the HOMO and LUMO for the neutral form and HOMO, SOMO, and LUMO for the cationic and anionic forms in dielectric (Figure 6) and explicit water (Figure 7). One distinctive feature of the LUMO of neutral BH_4 calculated in either dielectric or water is that it resembles the LUMO of the gas-phase cation rather than the LUMO of the gas-phase neutral BH_4. There is little difference between the HOMO of neutral BH_4 and the SOMO of the cation (dielectric and water), and the same holds for the LUMO. However, the HOMO of the cation (explicit water) shows different polarization the of α and β electrons: The α electron is localized mainly on the hydroxy tail of BH_4, while the β electron is localized on parts of the two rings of BH_4 containing the N^1 and N^8 atoms. In contrast, the SOMO of the anion in dielectric are very similar to the SOMO of the gas-phase BH_4 anion (i.e., localized near/on the pyrimidine ring), while the SOMO in water is mostly localized on the tail of BH_4, probably due to specific interactions with water molecules. The α and β electrons in the LUMO of the anion have different polarizations in water and similar polarizations in dielectric. This result demonstrates the limitation of using dielectric calculations as a substitute for an explicit solvent environment.

Protein Environment. We finally calculated the IP and EA of BH_4 docked in the active site of chains A and B of the iNOSoxy dimer. Figure 8 shows that in this particular configuration of the enzyme there are slightly different chemical environments for BH_4 docked to chain A (top panel) and chain B (bottom panel). One important feature of cofactor docking to NOS is that the carboxylic oxygen of one propionate group of heme makes bifurcated hydrogen bonds (Figure 8) with H^3 (0.192 nm in chain A and 0.188 nm in chain B) and one hydrogen atom of the NH_2 group of BH_4 (0.178 nm in chain A and 0.189 nm in chain B). Another distinctive feature is the sandwich arrangement (π-stacking) that BH_4, Trp^{463}, and Arg^{199} form (vide supra). The distance between BH_4 and Trp^{463} is 0.375 nm in chain A and 0.381 nm in chain B. The interactions of BH_4 with heme, the π-stacking residues (Trp^{463} and Arg^{199}), and Arg^{381} seem to be critical for the function of the cofactor. Tetrahydrobiopterin bound to chain A makes nine hydrogen bonds (Figure 8, top panel): Four hydrogen bonds are made with water molecules, while the other five hydrogen bonds are made with P_{450} $heme_A$, Ile^{462A}, Trp,^{463A} and Ser^{118A}. Tetrahydrobiopterin bound to chain B makes seven hydrogen bonds (Figure 8, bottom panel): Three hydrogen bonds are made with water molecules, and the remaining four hydrogen bonds are made with P_{450} $heme_B$, Ile^{462B}, Arg^{381B}, and Ser^{118B}.

Figure 9 shows the HOMO and LUMO of the neutral, and HOMO, SOMO, and LUMO of the cation and anion BH_4 bound to chain A (left panels) and chain B (right panels). As in the case of BH_4 solvated in water, the HOMO of the neutral BH_4 and the SOMO of the cation are similar and spread over the two rings of BH_4. In contrast, the occupied SOMOs of the anion (slightly different for chains A and B but similar with the LUMO of neutral BH_4) are localized near the BH_4 hydroxy tail, probably because of the presence of the heme propionate group in the vicinity of the pyrimidine ring of BH_4. This should increase the electron repulsion if the unpaired electron is localized in this region; this interaction makes the anion even more unstable. However, the virtual SOMOs (which are slightly different for chains A and B) are mainly localized on the pyrimidine ring. The α and β electrons in the LUMO of the anion have different polarizations, as is the case of BH_4 solvated in water.

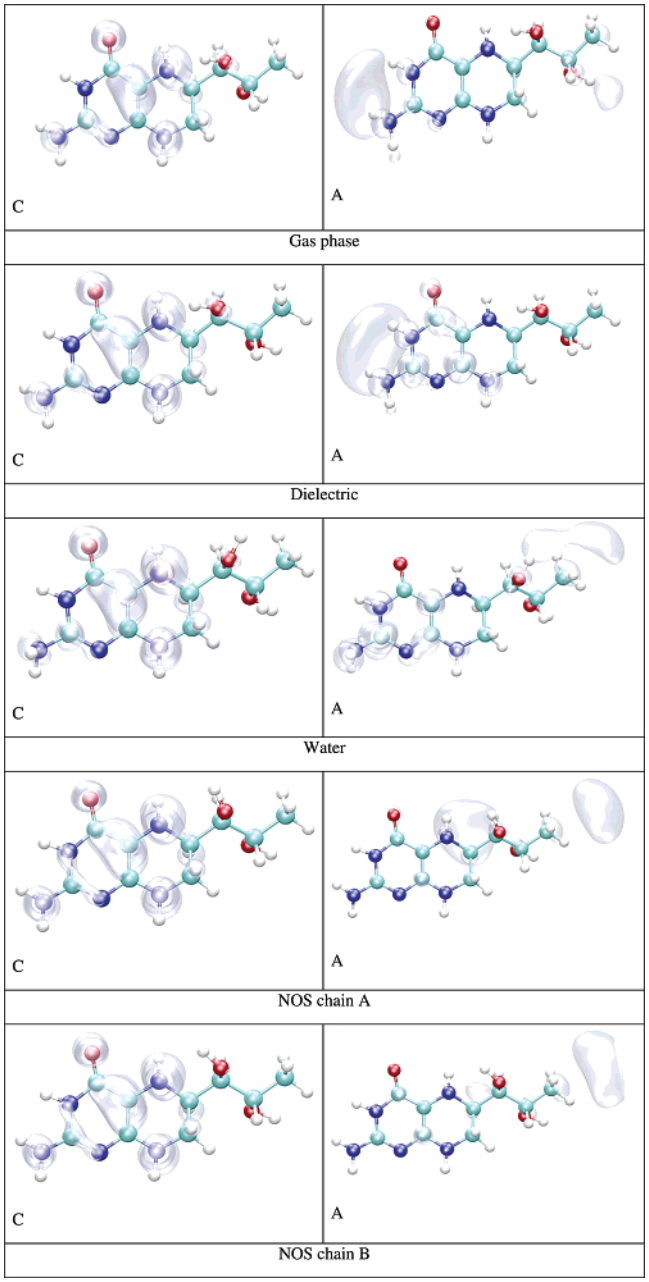

Figure 10. Spin densities for the BH_4 cation and anion calculated by density functional theory (B3LYP/6-31+G(d)) in the gas phase, dielectric, water and protein environments. The pictures have been obtained from CUBE Gaussian 98 files and displayed with the VMD and POV−Ray programs.

Figure 10 shows the spin densities of the cation (left panels) and the anion (right panels) species of BH_4 in the gas phase, solvated in dielectric and explicit water, and bound to chains A and B of the iNOSoxy dimer. While the cation's spin densities are very similar in all environments, being mostly localized at the junction between the pyrimidine and tetrahydropyrazine rings (including atoms N^5 and N^8), the spin densities found for the anion are much different. For the gas phase and dielectric the spin density is mostly localized on the side of the pyrimidine ring, whereas the spin density is localized on the tail for BH_4 in the explicit water and protein environments. Table 5 shows that the IP and EA of both BH_4 cofactors (chains A and B) are approximately 2 eV (IP) and 2.5 eV (EA) lower, respectively,

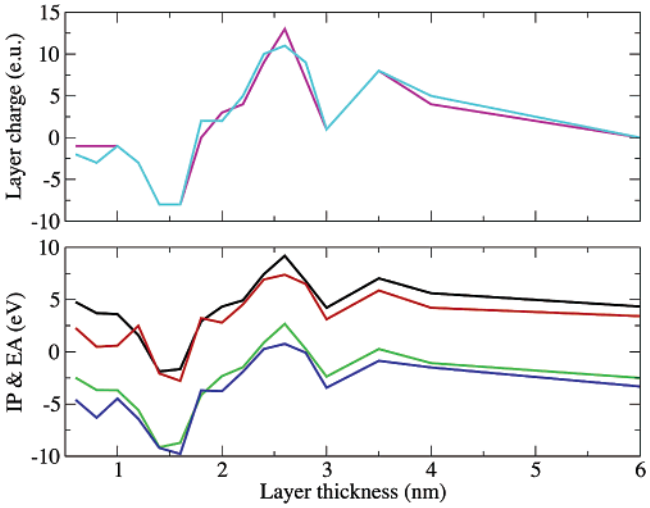

Figure 11. Bottom panel: Hypothetical change in the IP and EA of BH_4 due to the charge of a protein layer (of certain thickness) around BH_4. IP of BH_4 bound to chain A (black curve), IP of BH_4 bound to chain B (red curve), EA of BH_4 bound to chain A (green curve), EA of BH_4 bound to chain B (blue curve), Top panel: Variation of the charge on the protein layer (of certain thickness) around BH_4. Total charge on the protein layer around BH_4 bound to chain A (magenta curve), total charge on the protein layer around BH_4 bound to chain B (cyan curve).

in the protein environment than in either gas phase or explicit water. More importantly, there is a significant difference between the IP and the EA of BH_4 bound to chains A and B, even though their values in a vacuum (calculated for the geometries in the protein environment without the electric field of the point charges) differ little (Table 5). The ionization potential and electron affinity of BH_4 bound to chain B are 0.92 and 0.82 eV lower, respectively, than those calculated for BH_4 bound to chain A. Figure 11 (top panel) shows that charged amino acid residues of the iNOSoxy dimer make a multipole structure around BH_4 with a total charge (chain A BH_4 magenta curve, chain B BH_4 cyan curve) that varies dramatically as a function of the thickness of the layer. The multipole structure for a particular layer (hypothetical), which can have a net charge, demonstrates a fluctuation in the IP (chain A BH_4, black curve; chain B BH_4, red curve) and the EA (chain A BH_4, green curve; chain B BH_4, blue curve) as depicted in the bottom panel of Figure 11. This feature suggests that protein dynamics can dramatically alter the configuration of this multipole structure and thus substantially change the IP and EA of BH_4. Table 5 shows that the IP of BH_4 in protein environment is about half of its value in the gas phase and its EA is about 5 times smaller, which indicates that ionization becomes more likely and reduction less likely, in the protein environment than in the gas phase. We argue that during protein movement the multipole structure made of layers of charged residues around BH_4 can decrease the IP further such that BH_4 could donate an electron to the heme via the propionate bridge. For the anion to mediate the electron transfer it needs to acquire an electron from the reductase part of NOS before transferring it to the heme. If BH_4 has to act as a molecular switch and deliver an electron to heme in a timely manner, then it is less likely that the electron transfer would depend on another molecular event (i.e., the delivery of one electron from the reductase part of NOS to BH_4), which should be much slower. It also should be noted that the negatively charged propionate localizes the SOMO of BH_4 anion on its tail, that is, on the opposite side of the cofactor.

Conclusions

Our density functional theory calculations show that the electronic properties of BH_4 such as IP and EA are not very sensitive to conformational changes, but rather they change dramatically in the presence of an external electric field. Calculations of the IP and EA show that in the gas phase, in water, and in an energy-minimized protein environment the neutral BH_4 is the most stable species. The anion is more stable than the cation in all environments. An average polarization of water (provided in the form of a polarizable dielectric) makes the anion the most stable species in solution. The cation, however, is still 4.8 eV less stable, making the one-electron oxidation of BH_4 in solution difficult. The specific docking of BH_4 in iNOSoxy (i.e., in the vicinity of P_{450} heme with its pyrimidine ring next to a heme propionate group) may favor the cation as an electron-transfer mediator because the IP of BH_4 is then about half of what it is in the gas phase and the EA is about 5 times smaller. However, the susceptibility of the BH_4 wave function to external electric field fluctuations generated by moving charged residues should allow protein dynamics to produce proper configurations in which the cation (or the anion) becomes nearly as stable as or even more stable than the neutral BH_4 and thus facilitating the electron transfer to the heme. A paramagnetic species is observed during enzyme turnover, but there is no experimental procedure to distinguish whether an anion or a cation is involved in the electron transfer because both are radical species and produce the same electron spin resonance spectrum.

Acknowledgment. This work was supported by the National Institutes of Health (Grant No. 1R15GM070469-01), the Department of Energy (Grant No. DE-FG02-03ER15462), the National Center for Supercomputer Applications at the University of Illinois, and the Ohio Supercomputer Center.

Supporting Information Available: Table with calculated vibrational frequencies of tetrahydrobiopterin. This material is available free of charge via the Internet at http://pubs.acs.org.

References and Notes

(1) Wei, C.-C.; Crane, B. R.; Stuehr, D. J. *Chem. Rev.* **2003**, *103*, 2365.
(2) Eberlein, G.; Bruice, T. C.; Lazarus, R. A.; Henrie, R.; Benkovic, S. J. *J. Am. Chem. Soc.* **1984**, *106*, 7916.
(3) Davis, M. D.; Kaufman, S.; Milstien, S. *Eur. J. Biochem.* **1988**, *173*, 345.
(4) Vasquez-Vivar, J.; Whitsett, J.; Martasek, P.; Hogg, N.; Kalyanaraman, B. *Free Radical Biol. Med.* **2001**, *31*, 975.
(5) Milstien, S.; Katusic, Z. *Biochem. Biophys. Res. Commun.* **1999**, *263*, 681.
(6) Komori, Y.; Hyun, J.; Chiang, K.; Fukuto, J. M. *J. Biochem. (Tokyo)* **1995**, *117*, 923.
(7) Toth, M.; Kukor, Z.; Valent, S. *Mol. Hum. Reprod.* **2002**, *8*, 271.
(8) Curtius, H. C.; Heintel, D.; Ghisla, S.; Kuster, T.; Leimbacher, W.; Niederwieser, A. *Eur. J. Biochem.* **1985**, *148*, 413.
(9) Moad, G.; Luthy, C. L.; Benkovic, P. A.; Benkovic, S. J. *J. Am. Chem. Soc.* **1979**, *101*, 6068.
(10) Lazarus, R. A.; Wallick, D. E.; Dietrich, R. F.; Gottschall, D. W.; Benkovic, S. J.; Gaffney, B. J.; Shiman, R. *Fed. Proc.* **1982**, *41*, 2605.
(11) Fitzpatrick, P. F. *Annu. Rev. Biochem.* **1999**, *68*, 355.
(12) Flatmark, T.; Stevens, R. C. *Chem. Rev.* **1999**, *99*, 2137.
(13) Kappock, T. J.; Caradonna, J. P. *Chem. Rev.* **1996**, *96*, 2659.
(14) Gorren, A. C.; Mayer, B. *Curr. Drug Metab.* **2002**, *3*, 133.
(15) Wei, C.; Wang, Z.; Meade, A.; McDonald, J.; Stuehr, D. *J. Inorg. Biochem.* **2002**, *91*, 618.
(16) Becke, A. D. *Phys. Rev. A* **1988**, *38*, 3098.
(17) Lee, C.; Yang, W.; Parr, R. G. *Phys. Rev. B.* **1988**, *37*, 785.
(18) Moller, C.; Plesset, M. S. *Phys. Rev.* **1934**, *46*, 618.
(19) Head-Gordon, M.; Pople, J. A.; Frisch, M. J. *Chem. Phys. Lett.* **1988**, *153*, 503.
(20) Frisch, M. J.; Head-Gordon, M.; Pople, J. A. *Chem. Phys. Lett.* **1990**, *166*, 275.

(21) Frisch, M. J.; Head-Gordon, M.; Pople, J. A. *Chem. Phys. Lett.* **1990**, *166*, 281.

(22) Head-Gordon, M.; Head-Gordon, T. *Chem. Phys. Lett.* **1994**, *220*, 122.

(23) Saebo, S.; Almlof, J. *Chem. Phys. Lett.* **1989**, *154*, 83.

(24) Jorgensen, W.; Tirado-Rives, J. *J. Am. Chem. Soc.* **1988**, *110*, 1657.

(25) Besler, B. H.; Merz, K. M. J.; Kollman, P. A. *J. Comput. Chem.* **1990**, *11*, 431.

(26) Frisch, M. J.; Trucks, G. W.; Schlegel, H. B.; Scuseria, G. E.; Robb, M. A.; Cheeseman, J. R.; Zakrzewski, V. G.; Montgomery, J. A., Jr.; Stratmann, R. E.; Burant, J. C.; Dapprich, S.; Millam, J. M.; Daniels, A. D.; Kudin, K. N.; Strain, M. C.; Farkas, O.; Tomasi, J.; Barone, V.; Cossi, M.; Cammi, R.; Mennucci, B.; Pomelli, C.; Adamo, C.; Clifford, S.; Ochterski, J.; Petersson, G. A.; Ayala, P. Y.; Cui, Q.; Morokuma, K.; Malick, D. K.; Rabuck, A. D.; Raghavachari, K.; Foresman, J. B.; Cioslowski, J.; Ortiz, J. V.; Stefanov, B. B.; Liu, G.; Liashenko, A.; Piskorz, P.; Komaromi, I.; Gomperts, R.; Martin, R. L.; Fox, D. J.; Keith, T.; Al-Laham, M. A.; Peng, C. Y.; Nanayakkara, A.; Gonzalez, C.; Challacombe, M.; Gill, P. M. W.; Johnson, B. G.; Chen, W.; Wong, M. W.; Andres, J. L.; Head-Gordon, M.; Replogle, E. S.; Pople, J. A. *Gaussian 98*, revision A.11; Gaussian, Inc.: Pittsburgh, PA, 1998.

(27) Barone, V.; Cossi, M. *J. Phys. Chem. A* **1998**, *102*, 1995.

(28) Jorgensen, W. L.; Chandrasekhar, J.; Madura, J. D. *J. Chem. Phys.* **1983**, *79*, 926.

(29) Humphrey, W.; Dalke, A.; Schulten, K. *J. Mol. Graphics* **1996**, *14*, 33.

(30) Buck, D. K. *Persitance of Vision Racetracer*, version 3.6; Persistence of Vision Pty. Ltd.: Williamstown, Victoria, Australia, 2004.

(31) Lindahl, E.; Hess, B.; van der Spoel, D. *J. Mol. Model.* **2001**, *7*, 306

(32) Ryckaert, J. P.; Bellemans, A. *Faraday Discuss. Chem. Soc.* **1978**, *66*, 95.

(33) Shy, J.; Gogonea, V. OPLS Molecular Mechanics Force Field for P450 Heme. Presented at ACS Meeting-in-Miniature, Baldwin-Wallace College, Cleveland, OH, 2005.

(34) Li, H.; Raman, C. S.; Glaser, C. B.; Blasko, E.; Young, T. A.; Parkinson, J. F.; Whitlow, M.; Poulos, T. L. *J. Biol. Chem.* **1999**, *274*, 21276.

(35) Wei, C.-C.; Wang, Z.-Q.; Arvai, A. S.; Hemann, C.; Hille, R.; Getzoff, E. D.; Stuehr, D. J. *Biochemistry* **2003**, *42*, 1969.

(36) Breneman, C. M.; Wiberg, K. B. *J. Comput. Chem.* **1990**, *11*, 361.

(37) Raman, C. S.; Li, H.; Martasek, P.; Kral, V.; Masters, B. S. S. *Cell* **1998**, *95*, 939.

(38) Shy, J.; Gogonea, V. OPLS Molecular Mechanics Force Field for $[Zn(Cys)_4]^{2-}$ Complex. Unpublished work.

(39) Gorren, A. C. F.; Kungl, A. J.; Schmidt, K.; Werner, E. R.; Mayer, B. *Nitric Oxide* **2001**, *5*, 176.

(40) Damm, W.; Frontera, A.; Tirado-Rieves, J.; Jorgensen, W. *J. Comput. Chem.* **1997**, *18*, 1955.